Journal of Nuclear Materials 379 (2008) 54–58

Contents lists available at ScienceDirect

Journal of Nuclear Materials

journal homepage: www.elsevier.com/locate/jnucmat

The passivity of Type 316L stainless steel in borate buffer solution

Igor Nicic, Digby D. Macdonald *

Center for Electrochemical Science and Technology, Department of Materials Science and Engineering, Pennsylvania State University, University Park, PA 16802, United States

A B S T R A C T

The passivity of Type 316 SS in borate buffer solution (pH 8.35), in the steady-state, has been explored using a variety of electrochemical techniques, including potentiostatic polarization, Mott Schottky analysis, and electrochemical impedance spectroscopy. The study shows that the passive film is an n-type semiconductor with a donor density that is essentially independent of voltage across the passive state. The passive current density is also found to be voltage-independent, but the thickness of the barrier layer depends linearly on the applied voltage. These observations are consistent with the predictions of the Point Defect Model, noting that the point defects within the barrier layer of the passive film are metal interstitials or oxygen vacancies, or both. No evidence for p-type behavior was obtained, indicating that cation vacancies do not have a significant population density in the film compared with the two donors (cation interstitials and oxygen vacancies).

1. Introduction

Type 316L SS is a corrosion resistant alloy in its own right, for which a great deal of data exists. Accordingly, in many respects it is an ideal material for testing various models for the passive state and it is for this purpose that the current study was performed.

In this paper, electrochemical impedance spectroscopic (EIS) and Mott–Schottky (M–S) analysis of Type 316L SS have been performed. The ultimate goal of the study is to model experimental data within the point defect model and extract parameters that would enable us to predict corrosion damage under any given set of conditions. This report includes determination of the passive region for 316L SS in 0.2 M borate buffer (pH 8.35), measurement of steady state current for the region of passive film formation, validation of the electrochemical impedance data using the Kramers–Kronig transforms, determination of the semiconductor character and estimation of the dopant levels in the passive film, and estimation of the film thickness as a function of the formation potential. A more comprehensive analysis of the impedance data by optimization of the Point Defect Model will be published at a later date in Part II of this series.

2. Experimental

Electrochemical experiments were carried out on an EG&G flat cell. The working electrode was 3/8″ diameter 316L stainless steel (McMaster-Carr) cylinder mounted in resin with 0.385 cm^2 exposed to solution. The electrode surface was polished to a mirror finish with 1200 SiC paper and then further polished with 1 μm and 0.3 μm alumina. After polishing, the electrode was sonicated for 20 min in deionized water (18 $M\Omega\,cm^{-1}$, mili-Q) and then rinsed with copious amounts of water to remove any alumina. A borate buffer solution was made from 0.2 M boric acid (Alfa-Aesar, 99.99%) and 3 M sodium hydroxide (Aldrich, 99.99%). The sodium hydroxide solution was added dropwise to the boric acid solution, while vigorously stirring, until a pH of 8.35 was achieved. Prior to the experiment, the solution was purged with ultrahigh pure argon (UHP, 99.999%) for two hours and during the experiment a slow flow of argon was maintained. Before potentiostatic film growth, the electrode was held at $-1V_{SCE}$ for 10 min to remove the native oxide film.

All electrochemical experiments were performed using a Solartron 1287 Electrochemical Interface and a Solartron1280 Frequency Response Analyzer. A polarization curve was obtained at a potential scan rate of 2 mV/s. Potentiostatic film growth was performed for 24 h to ensure that steady state was achieved. After each film growth period, electrochemical impedance measurements were performed. The frequency was scanned between 0.01 Hz and 100 kHz and with an excitation voltage of 10 mV (peak-to-peak). The electrochemical impedance data were collected for both the ascending and the descending potential directions. The Reference electrode in all experiments was a saturated calomel electrode (SCE) equipped with a double junction and a Luggin probe. Mott–Schottky experiments were done by measuring the frequency response at 500 Hz during a 50 mV/s negative potential scan from the formation potential to $-0.64V_{SCE}$. This method ensures that the defect concentrations and the film

* Corresponding author. Tel.: +1 814 863 7772; fax: +1 814 863 4718.
E-mail address: ddm2@psu.edu (D.D. Macdonald).

0022-3115/$ - see front matter © 2008 Elsevier B.V. All rights reserved.
doi:10.1016/j.jnucmat.2008.06.014

thickness remain 'frozen' at their formation values while the capacitance is being measured as a function of voltage.

3. Results and discussion

Fig. 1 shows the potentiodynamic curve for the 316L stainless steel electrode in 0.2 M borate buffer adjusted to the pH of 8.35. From the polarization curve, the passive range was determined to be from −0.7 V to >0.5 V versus the SCE reference electrode.

Four potentials within the passive region were chosen for oxide film growth and impedance analyses, −0.2 V, −0.1 V, 0 V and 0.1 V vs. SCE. Films were gown at each potential for 24 h to insure that the system was in steady state. Fig. 2 shows that the logarithm of the steady state current density remains constant as a function of the formation potential. This relationship is predicted by the Point Defect Model (PDM), provided that the dominant defect is an electron donor (oxygen vacancy or metal interstitial) and hence the barrier layer of the passive film is n-type in electronic character. We will see later in this paper that this prediction is confirmed experimentally, thereby providing strong evidence that the PDM provides a physico-chemically realistic description of the passive state on this alloy. Furthermore, the fact that a steady state is observed in the passive film thickness demonstrates that dissolution of the oxide layer takes place and must be taken into account [1]. The lack of hysteresis due to the potential direction is another feature of a steady state system.

Electrochemical impedance spectra were measured at different formation potentials in the passive region. Nyquist plots, in which the imaginary component of the impedance is plotted against the real component as a function of frequency, are shown in Fig. 3. As predicted by PDM, the complex plane plot in the low frequency region is a straight line (a 'constant phase' impedance) and is insensitive to the formation potential. The constant phase nature of the impedance at low frequencies is a consequence of defect transport in the oxide film being manly due to migration under the influence of the electric field (i.e., transport occurs via migration and not diffusion). The lack of sensitivity of the impedance locus to the applied formation potential is a manifestation of the electric field strength in the barrier layer being insensitive to the applied potential, which is one of the fundamental postulates underlying the PDM. This ensures that the driving force for the transport of defects across the barrier layer is independent of the applied voltage. Physically, the constant, applied voltage-independent field strength is attributed to the buffering effect of Esaki (band-to-band) tunneling of electrons and holes in the barrier layer [2,3]. Therefore, the data presented here provide

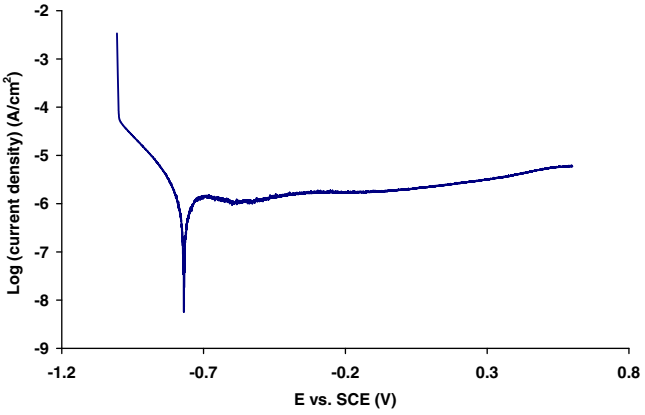

Fig. 1. Potentiodynamic polarization curve for Type 316L stainless steel electrode in 0.2 M borate buffer adjusted to pH of 8.35. The scan rate was 2 mV/s.

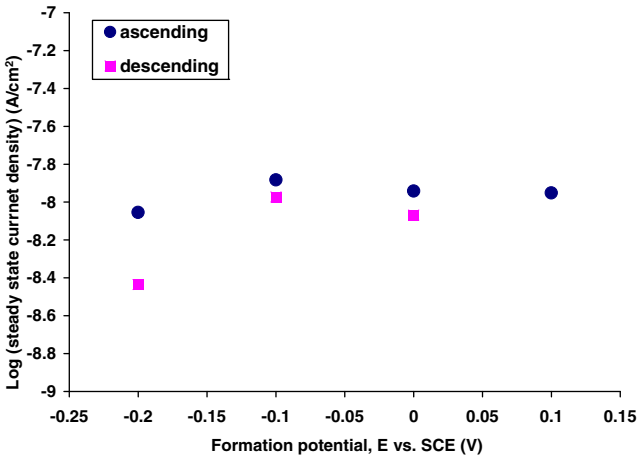

Fig. 2. Steady state (potentiostatic) current density for the Type 316L SS electrode in 0.2 M borate buffer (pH 8.35) showing the dependence on the oxide formation potential. Measurements were done in the following order: 1st −0.2 V, 2nd −0.1 V, 3rd 0 V, 4th 0.1 V, 5th 0 V, 6th −0.1 V, 7th −0.2 V. 1st though 4th are regarded as 'ascending' and 5th though 7th are regarded as 'descending' potential direction.

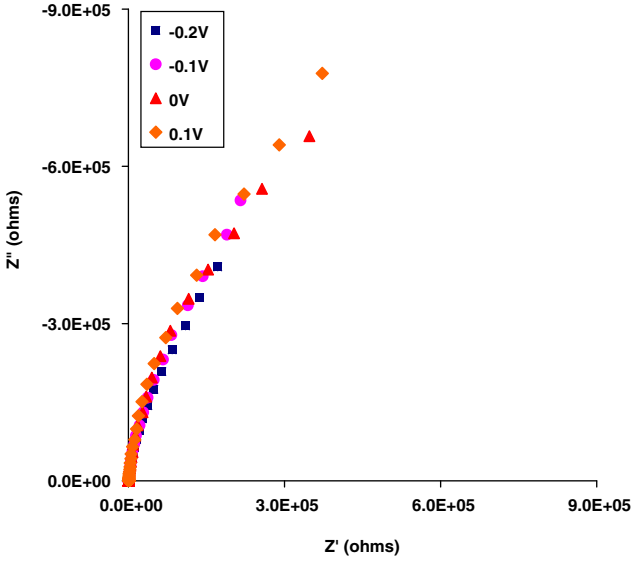

Fig. 3. Nyquist plot for the Type 316L SS in 0.2 M borate buffer (pH 8.35) measured at different oxide formation potential.

strong testimony to the constant electric field strength postulate of the PDM.

The stability of the system is crucial for the validity of EIS measurements. According to the constraints of Linear Systems Theory (LST), the steady–state interface should be independent of the direction of the frequency scan. Nyquist and Bode plots in Fig. 4 show that there is almost no hysteresis between high-to-low and low-to-high frequency sweeps and, therefore, confirm the validity of the data, at least with regard to the stability constraint.

Another way to validate the data and examine the system with respect to the linearity, causality and stability constraints of LST is the Kramers–Kronig transforms. K–K transforms, introduced in the 1920's by Kramers [4] and Kronig [5], describe transformations between the real and imaginary axes of a complex number that describes the properties of a system. Based on the assumption that the four physical conditions of causality, stability, linearity, and finiteness are fulfilled, the derivation of the K–K relations are a purely mathematical result and do not reflect any other physical

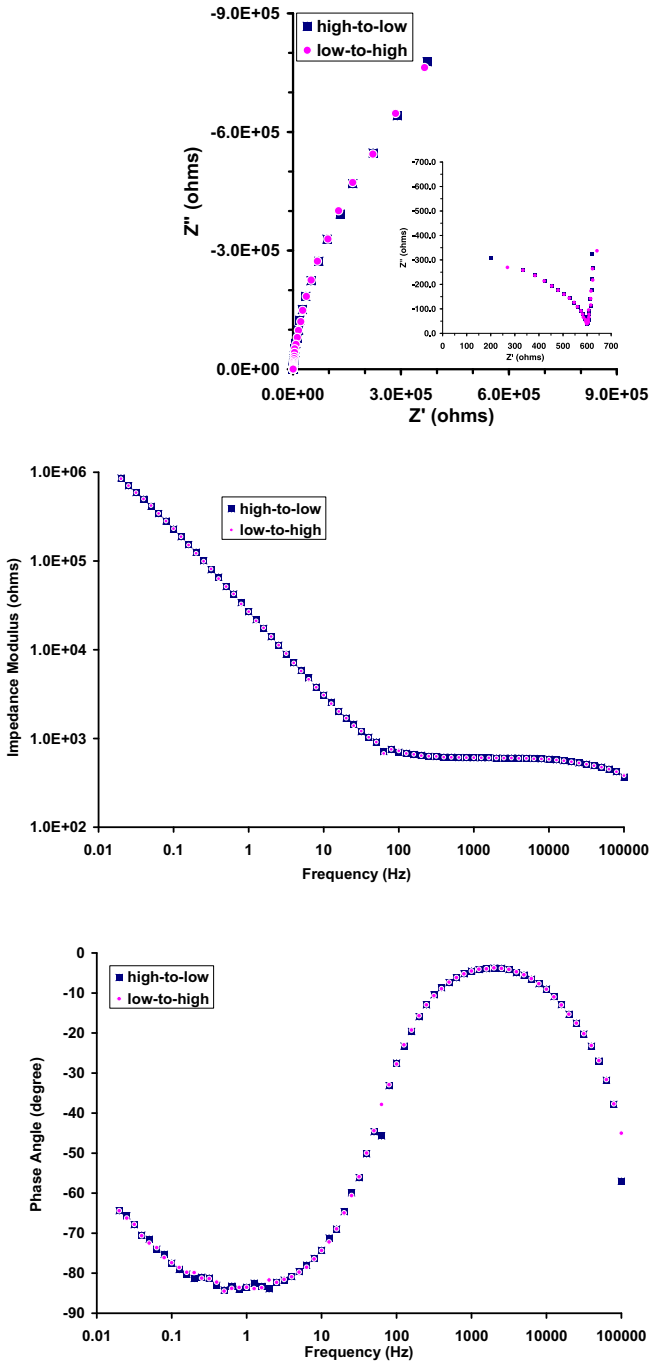

Fig. 4. Nyquist and bode plots for Type 316L SS at a potential of 0.1 V vs. SCE, measured first by scanning frequency from high to low and then immediately after scanning in opposite direction. The lack of hysteresis shows that the system is at steady state.

property or condition of the system. Thus, only those experimental data satisfying the above four conditions can be used to describe the properties of the systems in terms of LST and hence linear models. Linearity can be assured by choosing a sufficiently small perturbation, as is done in the experimental determination of the impedance function. The K–K transforms have been applied to the experimental impedance data by transforming the real axis into the imaginary axis and the imaginary axis into the real axis and then comparing the transformed quantities with the respective experimental data. Fig. 5 shows good agreement between the set of the impedance data and corresponding K–K transforms, demonstrating that the system satisfies the constraints of LST [6–10].

Mott–Schottky analysis has been employed to determine the semiconductor type and dopant density of the passive film. The equations for M–S analysis are:

$$\frac{1}{C_{sc}^2} = -\frac{2}{\hat{\varepsilon}\varepsilon_0 e N_A A^2}\left(V - V_{FB} - \frac{kT}{e}\right) \quad \text{p-type}, \tag{1}$$

$$\frac{1}{C_{sc}^2} = \frac{2}{\hat{\varepsilon}\varepsilon_0 e N_D A^2}\left(V - V_{FB} - \frac{kT}{e}\right) \quad \text{n-type}, \tag{2}$$

where $\hat{\varepsilon}$ is the dielectric constant of the oxide film ($\hat{\varepsilon} = 12$ [11–14]), A is the surface area of the electrode interface (cm^2), ε_0 is the vacuum permittivity, e is the charge of the electron (1.6×10^{-19} C), N_A and N_D are acceptor and donor density (cm^{-3}), and V_{FB} is the flat-band potential (V vs. SHE). The interfacial capacitance, C, is obtained from

$$C = -\frac{1}{\omega Z''}, \tag{3}$$

where Z'' is the imaginary component of the impedance and $\omega = 2\pi f$ is the angular frequency. Assuming that the capacitance of the double layer can be neglected, the measured capacitance C is equal to the space charge capacitance, C_{sc} Neglect of the double layer capacitance requires that the space charge specific capacitance be at least one to two orders lower than the specific double capacitance and must be significantly higher than the parallel geometric capacitance for this assumption to be valid. Insufficient data are available in the current case to judge the validity of the assumption that the space

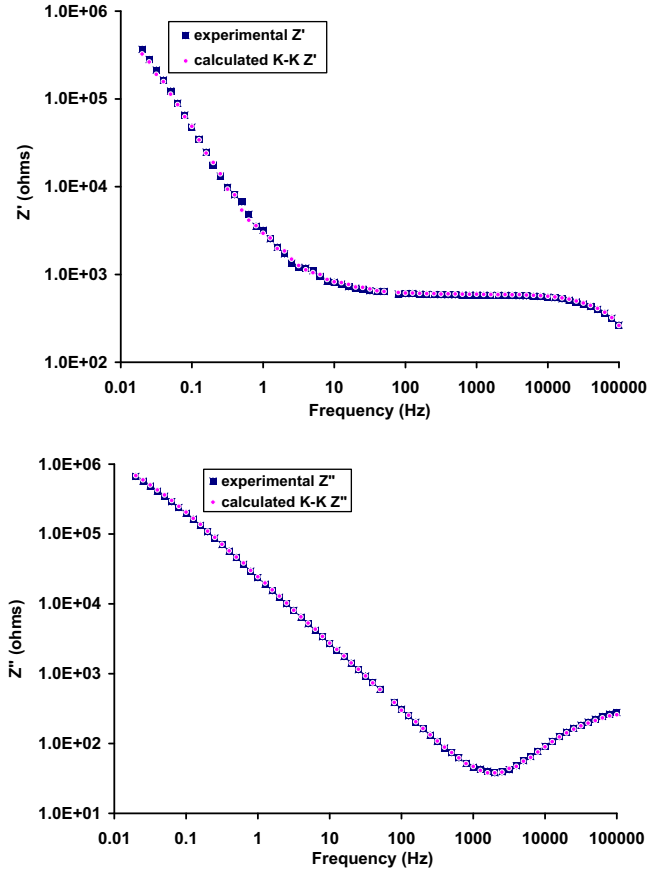

Fig. 5. Kramers–Kronig transforms of EIS data for the Type 316L SS in 0.2 M borate buffer (pH 8.35) at 0 V vs. SCE. The good agreement between the experimental and the transformed data demonstrates that the system obey the rules of the LST.

charge capacitance can be reasonably approximated by the measured capacitance.

The impedance data presented in this paper are not analyzed in the present paper, but the optimization of the Point Defect Model on the data will be reported at a later date. Optimization will yield numerical values for various model parameters that will enable prediction of both steady-state and dynamic properties of the passive state on the alloy and hence will permit the prediction of transients in the passive current density and film thickness in response to changes in the state of polarization.

Classical M–S analysis [13] also assumes that the donor density is uniform throughout the oxide film. It has been shown (in previous studies [13,15–17]) that these assumptions usually do not hold, thus M–S analyses in this paper should be regarded as semi quantitative. Fig. 6 represents typical C^{-2} vs. V plot for a passive film formed on Type 316L SS in 0.2 M borate buffer (pH 8.35) at a formation voltage of $0.1V_{SCE}$ and at room temperature. The impedance was measured at a frequency of the 500 Hz, while sweeping the potential in the negative direction from the formation potential with a scan rate of 50 mV/s. The relatively high scan rate is employed so that, during the measurement, the thickness, vacancy structure, and vacancy concentrations are 'frozen' and only the electronic structure responds to the changing voltage.

Fig. 7 displays negative slopes, indicative that n-type semiconductor behavior exists at all formation potentials. From the linear part of the slopes a donor density can be estimated. The dopant density calculated with this method indicates the density close to the metal/film interface, where the concentrations of oxygen vacancies and metal interstitials are predicted to be highest. Fig. 8 displays the donor density as a function of the formation potential, calculated for both ascending and descending film growth. Similar values for the donor density have been observed by Ferreira et al in Ref. 11, and the tendency of the donor density to decrease with increasing potential has been previously reported in Refs. [12,13].

Fig. 9 shows a linear relationship between the thickness of the oxide film and the formation potential. The film thickness was calculated from the capacitance measured at 500 Hz after each 24 h constant potential growth. It is assumed that, at this frequency, the electrochemical impedance is largely capacitive in nature, with the measured capacitance being almost independent of frequency.

The parallel plate expression was used for calculating the steady state film thickness from the measured capacitance:

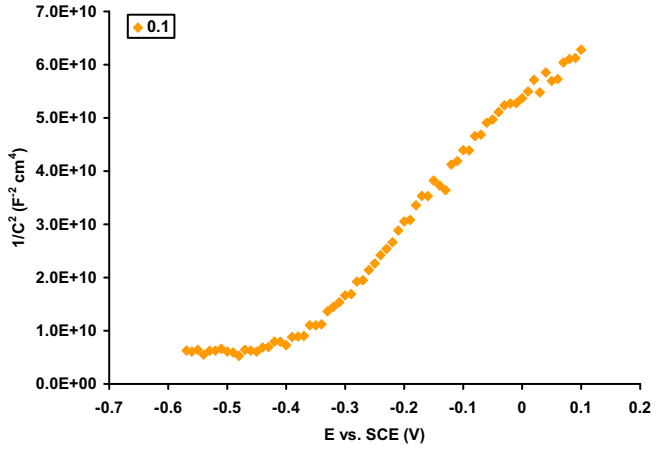

Fig. 6. Mott–Schottky plot for Type 316L SS passivated for 24 hours at a formation potential of 0.1 V vs. SCE. The impedance was measured at a frequency of the 500 Hz, while sweeping the potential in negative direction from the formation potential at a voltage scan rate of 50 mV/s.

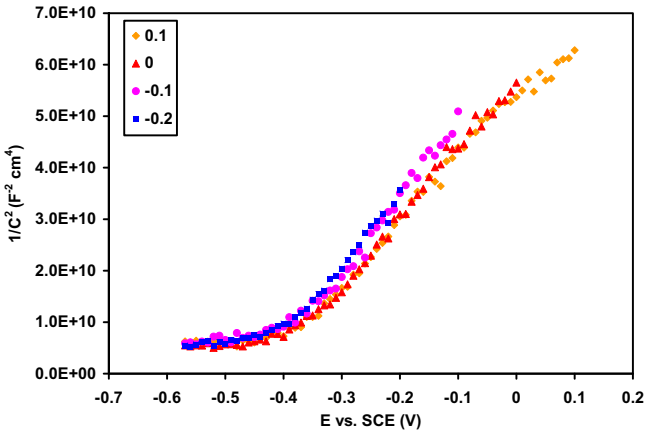

Fig. 7. Mott–Schottky plot for Type 316L SS passivated for 24 h at a formation potentials of –0.2 V, –0.1 V, 0 V and 0.1 V vs. SCE. The impedance was measured at a frequency of the 500 Hz, while sweeping the potential in negative direction from the formation potential at a voltage scan rate of 50 mV/s.

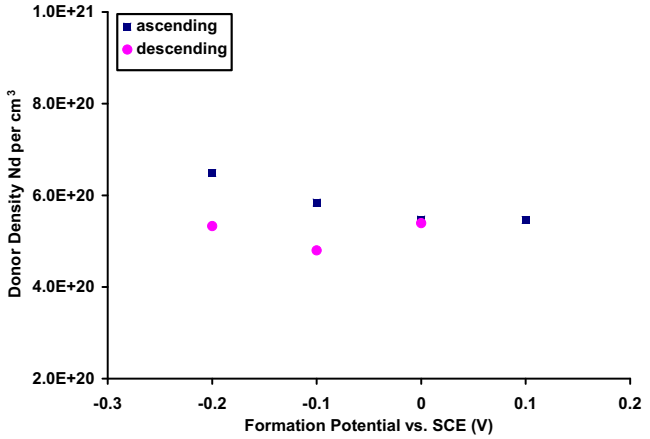

Fig. 8. Donor density for the barrier layer of the passive film on Type 316L SS at ambient temperature (23 °C) calculated from M–S plots as a function of formation potential. In our study, films were grown for 24 h in the following order: 1st −0.2 V, 2nd −0.1 V, 3rd 0 V, 4th 0.1 V, 5th 0 V, 6th −0.1 V, 7th −0.2 V. 1st though 4th are regarded as 'ascending' and 5th to 7th are regarded as 'descending'.

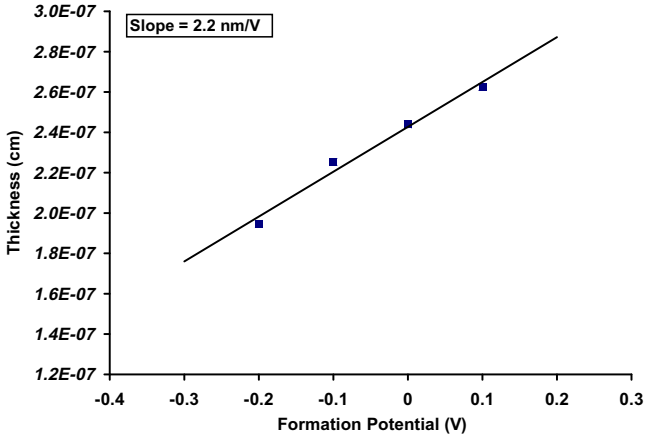

Fig. 9. Average film thickness as a function of the formation potential. Thickness was measured after each 24 h film growth.

$$L_{ss} = \frac{\hat{\varepsilon}\varepsilon^0}{C}. \quad (4)$$

The calculated thickness ranges from about 1.9 nm at $-0.2V_{sce}$ to 2.6 nm at $0.1V_{sce}$. These values of the thickness are considered to be eminently realistic. The slope extracted from Fig. 9 is 2.2 nm/V, which is in good agreement with the 1.9–2.5 nm/V normally found for oxide formation on metals and alloys at and near ambient temperature [18].

The findings of this study demonstrate that the passive state on Type 316 SS confirms to the predictions of the Point Defect Model and hence that this model may be used to predict the general corrosion behavior over the extended periods of time that characterize high level nuclear waste repositories. In particular, the passive current density may be used to calculate the general corrosion rate using the formula

$$\frac{dL}{dt} = \frac{\bar{M}}{\bar{z}F\rho} i_p, \quad (5)$$

where $\bar{M}$ and $\bar{z}$ are the composition-averaged atomic weight and oxidation number, respectively, ρ is the density of the steel, and i_p is the passive current density. Noting that

$$\bar{M} = \chi_{Fe}M_{Fe} + \chi_{Cr}M_{Cr} + \chi_{Ni}M_{Ni} + \chi_{Mo}M_{Mo} \quad (6)$$

and

$$\bar{z} = \chi_{Fe}z_{Fe} + \chi_{Cr}z_{Cr} + \chi_{Ni}z_{Ni} + \chi_{Mo}z_{Mo}, \quad (7)$$

where χ_i is the atom fraction, M_i is the atomic weight, and z_i is the oxidation number of element i in the steel, then the rate of penetration of general corrosion is readily calculated. Thus, taking a generic Type 316 L stainless steel as having a composition of 71.5 wt.% Fe, 18 wt.% Cr, 8 wt.% Ni, and 2.5 wt.% Mo, we obtain that χ_{Fe}, χ_{Cr}, χ_{Ni}, χ_{Mo} are 0.7157, 0.1935, 0.0762, 0.0146, respectively. The composition averaged atomic weight of the steel, as calculated from Eq. (6), is 55.905 g. Likewise, noting that z_{Fe}, z_{Cr}, z_{Ni}, and z_{Mo} are 2, 3, 2, and 6, respectively, the composition-averaged oxidation number is found from Eq. (7) to be 2.3721. Taking the density of Type 316 SS as 7.99 g/cm^3, the corrosion rate calculated from Eq. (5) corresponding to a passive current density of 10^{-8} A/cm^2 (Fig. 2) is 3.06×10^{-13} cm/s or 0.096 μm/year. Accordingly, over a one million year storage period, about 10 cm of steel might be expected to be lost due to general corrosion, if the conditions corresponded to those assumed in this calculation.

4. Summary and conclusions

Potentiodynamic polarization studies demonstrate that Type 316L SS displays a wide passive range in borate buffer solution at ambient temperature (23 °C). Under steady-state conditions, the passive current is found to be independent of voltage and the film thickness is found to increase linearly with applied voltage with an anodizing constant of 2.2 nm/V. Impedance data were collected and validated by Kramers–Kronig transformation. These data will be analyzed in terms of the mechanism of passive film formation, as described by the Point Defect Model in Part II of this series. Mott–Schottky analyses were used to estimate the donor concentration of the barrier layer of the passive film. Although some question exists as to whether the necessary conditions for M–S analysis were fulfilled in the present study, the passive films are clearly n-type in electronic character and reasonable values for the donor density as a function of voltage were obtained. The donor density was found to be essentially independent of film formation voltage with a slight trend for the density to decrease with increasing voltage. The data obtained in this study demonstrate that the passive state on Type 316L SS is well accounted for by the Point Defect Model, with this alloy joining a long list of other alloys and metals that have been successfully interpreted in terms of this model [2,19–23].

Acknowledgements

Support by the Science & Technology Program of the Office of the Chief Scientist (OCS), Office of Civilian Radioactive Waste Management (OCRWM), U.S. Department of Energy (DOE), is gratefully acknowledged. The work was performed under the Corrosion and Materials Performance Cooperative, DOE Cooperative Agreement No: DE-FC28-04RW12252. The views, opinions, findings, and conclusions or recommendations of authors expressed herein do not necessarily state or reflect those of the DOE/OCRWM/OCS.

References

[1] D.D. Macdonald, J. Electrochem. Soc. 139 (1992) 3434.
[2] E. Sikora, D.D. Macdonald, Electrochim. Acta 48 (2002) 69.
[3] D.D. Macdonald, S.I. Smedley, Electrochim. Acta 35 (1990) 1949.
[4] H. Kramers, Phyzik. Z. 30 (1929) 521.
[5] R. de, L. Kronig, J. Opt. Soc. Am. 12 (1926).
[6] M. Urquidi-Macdonald, S. Real, D.D. Macdonald, J. Electrochem. Soc. 133 (1986) C132.
[7] M. Urquidi-Macdonald, S. Real, D.D. Macdonald, J. Electrochem. Soc. 133 (1986) 2018.
[8] M. Urquidi-Macdonald, S. Real, D.D. Macdonald, Electrochim. Acta 35 (1990) 1559.
[9] D.D. Macdonald, M. Urquidi-Macdonald, S. Real, J. Electrochem. Soc. 134 (1987) C419.
[10] D.D. Macdonald, M. Urquidi-Macdonald, J. Electrochem. Soc. 137 (1990) 515.
[11] N.E. Hakiki, M. Da Cunha Belo, A.M.P. Simoes, M.G.S. Ferreira, J. Electrochem. Soc. 145 (1998) 3821.
[12] A. Di Paola, Electrochim. Acta 34 (1989) 203.
[13] U. Stimming, J.W. Schultze, Ber. Bunsenges. Phys. Chem. 79 (1976) 1206.
[14] F. Gaben, B. Vuillemin, R. Oltra, J. Electrochem. Soc. 151 (2004) B595.
[15] C. Wagner, Ber. Bunsenges. Phys. Chem. 77 (1973) 1090.
[16] A. Goossens, M. Vazquez, D.D. Macdonald, Electrochim. Acta 41 (1996) 35.
[17] D.D. Macdonald, E. Sikora, J. Sikora, Electrochim. Acta 43 (1998) 2851.
[18] L. Young, Anodic Oxide Films, Academic Press Inc., New York, 1961.
[19] J. Sikora, E. Sikora, D.D. Macdonald, Electrochim. Acta 45 (2000) 1875.
[20] D.D. Macdonald, A. Sun, N. Priyantha, P. Jayaweera, J. Electroanal. Chem. 572 (2004) 421.
[21] N. Priyantha, P. Jayaweera, D.D. Macdonald, A. Sun, J. Electroanal. Chem. 572 (2004) 409.
[22] J. Ai, Y. Chen, M. Urquidi-Macdonald, D.D. Macdonald, J. Electrochem. Soc. 154 (2007) C43.
[23] J. Ai, Y. Chen, M. Urquidi-Macdonald, D.D. Macdonald, J. Electrochem. Soc. 154 (2007) C52.